RSC Advances

PAPER

View Article Online
View Journal | View Issue

Cite this: *RSC Adv.*, 2017, **7**, 42083

Doping-template approach of porous-walled graphitic nanocages for superior performance anodes of lithium ion batteries†

Zhao Min Sheng,* Xin Jian Chang, Yu Hang Chen, Cheng Yang Hong, Na Na Li, Cheng Kang Chang, Run Ping Jia and Sheng Han*

Received 17th July 2017
Accepted 23rd August 2017

DOI: 10.1039/c7ra07859e

rsc.li/rsc-advances

In a template approach to porous-walled graphitic nanocages (PWGNC) with N-doping structure, nanopores have been equably and efficiently created in the shells of GNCs by partially removing N-doped templates, which replace some C atoms in the graphitic layers of the GNCs by *in situ* doping during thermal pyrolytic preparation of GNCs. Such created nanopores offer many efficient diffusion channels for fast distribution of the electrolyte and Li^+ (specific surface area and mesopore volume sharply rose 1100 *vs.* 700 $m^2\ g^{-1}$; 1.9 *vs.* 1 $cm^3\ g^{-1}$), leading to their hollow inner structure available even at elevated charge/discharge rates, which sharply enhances the performance of the PWGNC-based anode with charge–discharge rate increases (31% increase: 1200 *vs.* 917 mA h g^{-1} at current density of 0.2 A g^{-1}; 52% increase: 510 *vs.* 335 mA h g^{-1} at 5 A g^{-1}).

Lithium ion batteries (LIBs) are commercially successful energy storage devices, due to their high energy density, high operating voltage and long cycle life.[1–19] Its low cost, good electronic conductivity, moderate operation voltage and stability enable graphite to be the dominant anode material for the current LIBs, leading to many novel anodes prepared from advanced graphitic nanomaterials, such as carbon nanotubes (CNTs),[5,6] nanofibers (CNFs),[7] nanocages[2,9–12,17–20] and graphenes,[13–16,21,22] drawing great attention. However, their performance is still far from satisfactory, especially at a high charge–discharge rate (≥0.5 A g^{-1}), as graphite has a lower theoretical capacity of 372 mA h g^{-1}.[12–26] It should be noted that achieving high capacities at elevated charge/discharge rates is particularly challenging since the time available for ions to diffuse through the anode and intercalate is now significantly shorter.[13,22] Chemical doping is an effective strategy to enhance such performance by increasing electronic conductivity or active sites for Li^+ storage.[7,10,12–14,20] Additionally, photothermal-reduced graphene was reported to increase Li^+ diffusion channels by creating micrometer-scale open-pore structure in the graphene anodes.[13] Additionally, nanopores was created on the shells of carbon nanomaterials by template approach[3] or KOH activation,[4] which was reported to enhance diffusion of Li^+ and electrolyte.[3,4] Thus, an efficient method to equably create nanopores on shells of such materials might sharply enhance ions diffusion to improve the performance of the LIBs for high rate applications.

Here, we demonstrate a novel approach for the N-doped graphitic nanocage with a porous-walled shell. In such approach, nanopores have been equably and efficiently created in the shells of GNCs by partially removing N-doped templates, which replace some C atoms in the graphitic layers of the GNCs by *in situ* doping during thermal pyrolytic preparation of GNCs. Such created nanopores could offer many efficient diffusion channels for fast distribution of the electrolyte and Li^+, leading to their hollow inner structure available even at elevated charge/discharge rates. Thus, such N-doped porous-walled graphitic nanocage might be a superb electrode material towards high performance applications of LIBs.

For preparing graphitic nanocages with high specific surface area, core–shell nanoparticles were prepared by thermal pyrolyzing a gas mixture of nitrogen, ammonia, acetylene and iron pentacarbonyl at 550–1050 °C. The typical flow rates were 80 L h^{-1} for nitrogen, 30 mL min^{-1} for ammonia and 10 mL min^{-1} for acetylene, and those gases flowed through the liquid iron pentacarbonyl to add the chemical into the gas mixture. After thermal pyrolysis, core–shell nanoparticles were collected at the other end of the quartz tube. To remove the cores, the nanoparticles were stirred in mixed acid ($HCl : HNO_3$ = 10 : 1) at 80 °C for 6 h and then such acid-treated samples were filtered and dried to obtain N-doped graphitic nanocages. For preparing PWGNCs, the nanocages were annealing in vacuum at 300 °C for 0.5 h to partially remove N-doping template, leading to the PWGNCs' yield of ~2 g per day.

School of Materials Science and Engineering, Shanghai Institute of Technology, Shanghai 201418, China. E-mail: zmsheng@sit.edu.cn; Hansheng654321@sina.com; Fax: +86-21-60873439

† Electronic supplementary information (ESI) available. See DOI: 10.1039/c7ra07859e

All samples were analyzed by X-ray diffractometer (XRD: Bruker D8 Advance, Bruker AXS, Germany), and high-resolution transmission electron microscopy (HRTEM: JEOL, JEM-2100F, Japan) and X-ray photoelectron spectroscopy (XPS). Nitrogen adsorption/desorption measurement of the carbon samples were carried out at 77 K (ASAP 2020, Micromeritics). CR2016-type coin cells were assembled in an argon-filled glove box to evaluate the electrochemical performance of PWGNCs-based electrodes. The PWGNCs-based working electrode was fabricated by a slurry coating procedure and the slurry was obtained by mixing active materials (GNCs), super-P carbon black and polyvinylidene fluoride (PVDF) at a weight ratio of 70 : 15 : 15 in *N*-methylpyrrolidinone (NMP), and then the slurry was coated on the Cu foil and dried at 100 °C under vacuum for 12 hours. In addition to the working electrode, pure lithium foil and porous polypropylene film (Celgard 2400) were used as counter electrode and separator, respectively, and $LiPF_6$ were dissolved in the solution with 1 : 1 : 1 ethylene carbonate (EC), diethyl carbonate (DEC) and dimethyl carbonate (DMC) by volume to prepare 1 M $LiPF_6$ electrolyte. After assembly, the cyclic voltammetry profiles and the galvanostatic charge–discharge measurements of the cells were carried out between 0.005 and 3 V (*vs.* Li^+/Li) at room temperature on a CHI 760E electrochemical workstation and a battery test system (LAND CT-2001A tester).

According to transmission electron microscope (TEM) images (Fig. 1a), the precursors of N-doped GNCs (NGNCs), which have been prepared by thermal pyrolysis at 750 °C, are 3–20 nm nanoparticles encapsulated by well-graphitized shells. The X-ray diffraction (XRD) result (Fig. 1b) indicates the core nanoparticles are Fe_3C. After acid-treatment, the ferrous cores were eliminated and only graphitic shells remained (Fig. 1c and d). In Fig. 1c, the (002) diffraction peaks of NGNCs prepared at 750 °C and their HRTEM image (Fig. 1d) indicate good graphitization of NGNC750. Due to altering thermal pyrolytic temperature, the wide peak of NGNC550 suggests its poor graphitization (Fig. 1c and S1a of ESI†) and narrow peak of NGNC1050 suggests its thick graphitic shells (>3 nm, Fig. 1c and S1b of ESI†). The HRTEM image of NGNC750 is shown in Fig. 1d: the diameters of NGNCs are ranged 3–20 nm and their graphitic shells are enclosed without distinguished nanopores. According to HRTEM image (Fig. 1e), a lot of nanopores have formed from annealing NGNCs in vacuum. Thus, porous-walled graphitic nanocages have been prepared.

To further investigate formation of porous-walled shells coming from annealing NGNCs in vacuum, prepared graphitic nanocages samples were measured by N_2 adsorption–desorption isotherms and X-ray photoelectron spectroscopy (XPS) and the results were shown in Fig. 2. Calculated from N_2 adsorption–desorption isotherms (Fig. 2a and S2a–d of ESI†), specific surface area (S_{BET}) (PWGNC750: 1100 $m^2\ g^{-1}$ *vs.* NGNC750: 700 $m^2\ g^{-1}$) and mesopore volume (PWGNC750: 1.9 $cm^3\ g^{-1}$ *vs.* NGNC750: 1 $cm^3\ g^{-1}$, Fig. S2d†) of the GNCs were sharply raised after partial removal of N-doping structure by annealing in vacuum at 300 °C, indicating nanopores have been created in the shell of GNCs by partially removing the N-doped template.

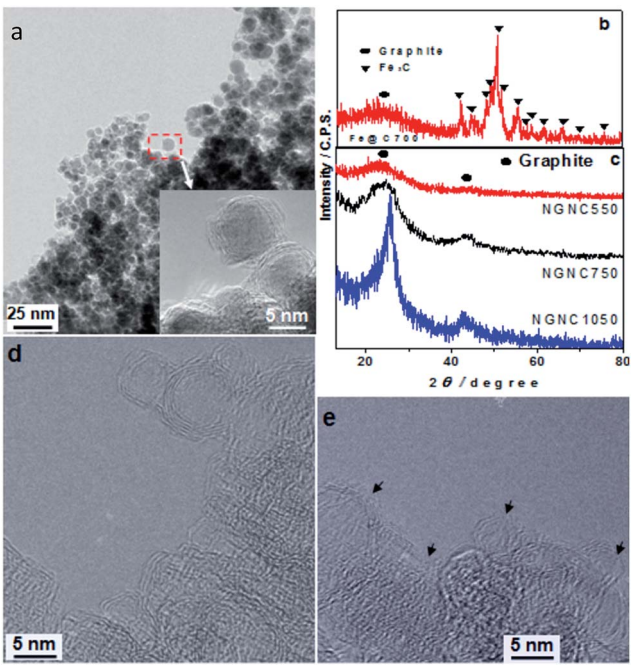

Fig. 1 TEM image (a) and XRD pattern (b) of the GNC-precursor (Fe@C750) prepared by thermal pyrolysis at 750 °C. XRD patterns (c) of N-doped GNC samples prepared from acid-treating the precursor. HRTEM images of N-doped GNCs before (d, NGNC750) and after (e, PWGNC750) removing doped templates (nanopores are arrowed).

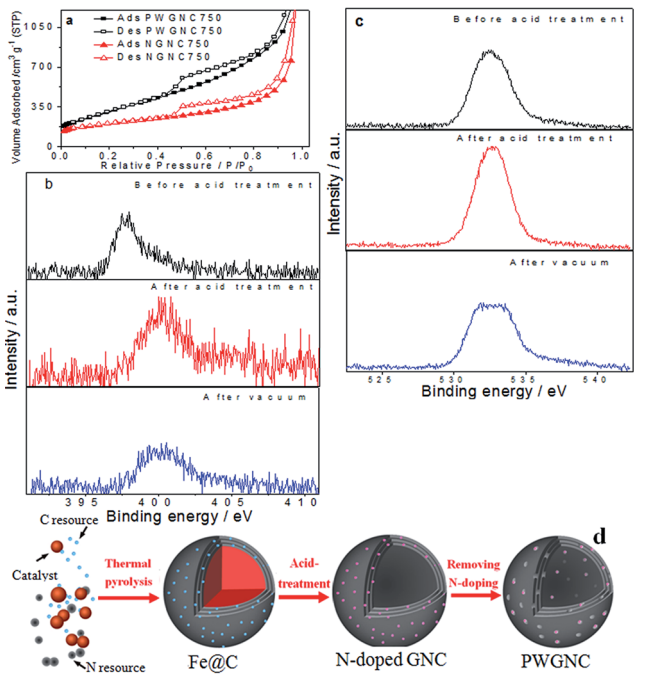

Fig. 2 N_2 adsorption/desorption isotherms (a) of the GNCs before and after removal of N-doping structure by 300 °C heat treatment in vacuum. XPS N 1s spectra (b) and O 1s spectra (c) of GNC-precursor (before acid treatment), NGNCs (after acid treatment) and PWGNCs (after annealing in vacuum). (d) Possible growing process of PWGNCs from doping-template approach.

According to XPS results (Fig. 2b), N atom contents of prepared Fe@C precursor was ~1.5 wt% and that of NGNC750 rose to ~3 wt%, because of removing ferrous cores by acid treatment; N atom contents of PWGNC750 was reduced to 2 wt%, due to partial removal of N-doped template by annealing in vacuum. The N 1s spectrum of Fe@C precursor prepared at 750 °C was located at ~398 eV corresponding to pyridinic nitrogen[10,11] and that of NGNC750 was shifted to ~402 eV, which might be caused by oxidation of N-doping structure in acid-treatment.[11] For investigating this oxidation process, O atom contents of prepared samples were also measured (Fe@C precursor: 7.5 wt%; NGNC750: 12 wt%; PWGNC750: 6 wt%) and shown in Fig. 2c. In XPS C 1s spectra (Fig. S2e†), the overall peak of the PWGNC750 became sharp. All XPS results indicate the N-doped GNCs were partially oxidized by acid treatment and the oxygen-containing functional groups were sharply removed due to annealing in vacuum.

The prepared PWGNC-based electrodes were assembled against Li foil in a two-electrode coin cell (CR2016) to evaluate their electrochemical performances (Fig. 3). Galvanostatic charge/discharge profiles of PWGNC750 at current density of 0.2 A g^{-1} for the 1st–5th cycles exhibited the typical shape of graphitic anodes: the PWGNC750-based anode delivered initial charge and discharge capacities of 1240 and 2300 mA h g^{-1}, respectively, with a first-cycle columbic efficiency (CE) of 54% (Fig. 3a). This low CE might be attributed to the formation of a solid electrolyte interface (SEI) film on the surface of the carbon materials.[12,15] Nevertheless, the CEs sharply increased to 87% in the sequent cycles (Fig. 3a), and then reached ~100%, with number of cycles increasing (Fig. 3d). Such results were consistent with the cyclic voltammetry (CV) profile (Fig. S3†). After the first cycle, the strong peak located at ~0.6 V disappeared, indicating the complete formation of SEI layer.

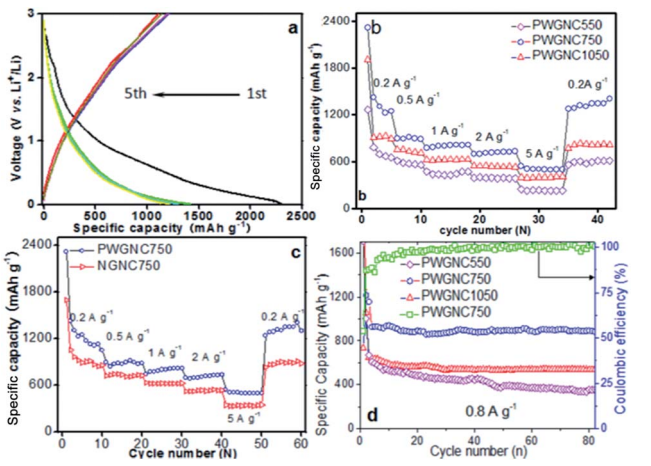

Fig. 3 Electrochemical performance of GNCs: (a) the galvanostatic charge–discharge profile of PWGNC750; charge–discharge cycling performances of PWGNCs (b), and performances of GNCs (c) before (NGNC750) and after (PWGNC750) removal of N-doping structure at different current densities from 0.2 A g^{-1} to 5 A g^{-1} at room temperature; cycling capability (d) of PWGNCs prepared at different temperature at 1 A g^{-1} (current densities).

To further verify performance of the PWGNC-based anodes for high rate applications, their rate capability behaviour was tested at different current densities. Such stepped-rate studies enable a better understanding of the anode performance, and more importantly, provide information of the repeatability of the electrode. PWGNC750-based electrode exhibited a higher capability than others (Fig. 3b): 1200 mA h g^{-1} at current density of 0.2 A g^{-1}; 930 mA h g^{-1} at 0.5 A g^{-1}; 850 mA h g^{-1} at 1 A g^{-1}; 735 mA h g^{-1} at 2 A g^{-1}; 510 mA h g^{-1} at 5 A g^{-1}. The low electrochemical performance (880 mA h g^{-1} at 0.2 A g^{-1}; 420 mA h g^{-1} at 5 A g^{-1}) of PWGNCs prepared by thermal pyrolysis at 1050 °C (PWGNC1050) might be caused by thickness of graphitic shells rising with synthetic temperature, which reduced both specific surface area (600 m^2 g^{-1}) and pore volume (0.9 cm^3 g^{-1}) of PWGNC1050 (Fig. S2c†). In order to obtain a clearer understanding of the extent of improvement, control tests were carried out, comparing with NGNC750 (N-doped GNCs prepared by acid-treatment without removal of doped template). As a result, capability of PWGNC-based electrode increased more, with current density rising (PWGNC750 *vs.* NGNC750: 1200 *vs.* 917 mA h g^{-1}, 30% increase at 0.2 A g^{-1}; 32% increase at 0.5 A g^{-1}; 35% increase at 1 A g^{-1}; 40% increase at 2 A g^{-1}; 50% increase at 5 A g^{-1}), indicating porous-walled graphitic shells of GNCs are very useful to enhance performance of PWGNC-based anode for the current LIBs at a high charge–discharge rate (Fig. 3c). For further investigating effect of porous-walled shells, AC impedance plots for NGNC750 and PWGNC750 were measured, and the results show porous-walled graphitic shells of GNCs sharply enhance diffusion of Li^+ and electrolyte (Fig. S4†).

Additionally, the discharge–charge cycling stability of PWGNC-based electrodes were measured at a current density of 1 A g^{-1} between 0.005 and 3 V (Fig. 3d). The electrodes prepared from well graphitized PWGNCs had good performance of cycling stability, and after 80 discharge–charge cycles, the performance reductions of PWGNC750 and PWGNC1050 were <4% and <6%, respectively. Despite high specific surface area of PWGNC550 (1040 m^2 g^{-1}, Fig. 2a), the performance of the poorly graphitized PWGNC550-based electrodes was poor: the discharge capacity was reduced from 600 to 360 mA h g^{-1} after 80 discharge–charge cycles. For further testing stability performance of NGNC750 and PWGNC750, 1000 discharge–charge cycles were carried out at current densities of 4 A g^{-1} (Fig. S4†). The performance reductions of PWGNC750 was less than that of NGNC750 during 1–200 cycles, and then performance of PWGNC750 became poor till 800 discharge–charge cycles was finished. However, the reversible capacity was over 250 mA h g^{-1} for PWGNC750, which was still high performance at current densities of 4 A g^{-1}, indicating good graphitization of GNCs could enhance their resistance to electrochemical corrosion as well as their capacitance.

How the present nanoporous wall of GNCs formed in vacuum-annealing is subject to discussion. According to TEM (Fig. 1d and e), N_2 adsorption–desorption isotherms (Fig. 2a) and XPS (Fig. 2b and c) results, the process of nanoporous wall formation was supposed (Fig. 2d). In the acid-treatment of Fe@C precursor, N-doping structure and the graphitic structure

next to the doping structure could be easily oxidized, leading to nanopores as well as oxygen-containing functional groups sharply increasing. Thus, their O atom contents rise from 7.5 to 12 wt% (Fig. 2c). However, those functional groups existed around the nanopores formed from the acid-treatment, which might block the nanopores. With vacuum-annealing leading to ~50% oxygen-containing functional groups were removed (O atom contents were reduced from 12 to 6 wt%; Fig. 2c), those nanopores might be open and their specific surface area sharply rose. As far as we know, reported N-doped graphitic nanomaterials with high specific surface area were rarely treated with both mix-acid treatment and annealing in vacuum, after doping. Doped graphene or graphene oxide samples from annealing was usually reported to directly prepare electrodes without further treatment,[13,15] and some N-doped graphene and nanoporous carbon prepared by chemical vapor deposition were prepared from only HCl[10,27] or HF[28] treatment to remove substrate or template. Although N-doped CNTs and CNFs might be treated with mix-acid to remove catalysts, such materials were prevented from their specific surface area sharply rising (usually <600 $m^2 g^{-1}$),[5–7] due to diffusion channels were hard to form on their thick graphitic layers, which was similar to the performance of the present thick-walled GNCs (NGNC1050). Hence, both mix-acid treatment and vacuum-annealing led to specific surface area of thin-walled N-doped GNCs (NGNC750) sharp increasing.

It is noticed that the good performance of the prepared PWGNC750 is apparently ascribed to it graphitic shells with highly nanoporous-walled structure. High nanoporosity of graphitic shells could effectively shorten diffusion route of Li^+ in the insertion/emersion process of the ions into the interlayer of the graphitic nanostructure of the prepared PWGNCs, which is demonstrated in Fig. S6.† Additionally, porous-walled shells might make inter-cage mesopores available. Thus, the readily accessed void space inside the cages acts as a reservoir for the electrolyte, leading to efficient Li^+ insertion into the carbon shells, and both outer and inner surface of the cages available for insertion/emersion process of Li^+. Moreover, position distribution of N-doped template-prepared nanopores is very homogeneous in the graphitic shells of PWGNCs, due to *in situ* N-doping in the graphitic shells during pyrolytic preparation of Fe@C precursors. Hence, more N-doping structure and interlayer of highly nanoporous-walled graphitic shells are available for storage of lithium to enhance the specific capacity. Such created nanopores could offer many efficient diffusion channels for fast distribution of the electrolyte and Li^+, which is supported by AC impedance results (Fig. S4†). Thus, such N-doped porous-walled graphitic nanocage might be a superb at high charge/discharge current density, leading to great improvement from NGNC750 to PWGNC750 (Fig. 3c and S4†).

Compared with currently reported carbon-anode materials for LIBs (current density of 0.2 A g^{-1}: <200 (CNTs),[5] 463.2 (graphene),[21] ~500 (hollow carbon nanoparticles),[3] 632.8 (N-doped carbon hollow spheres),[23] 862.2 (N-doped CNFs),[7] 817 (N-doped graphene)[9] and ~1020 (N-rich porous carbon)[11] mA h g^{-1}; 5 A g^{-1}: <200,[7] 297,[9] ~290 (N- and S-codoped graphene),[15] 304 (ref. 11) and 340 (N-doped GNCs)[12] mA h g^{-1}), electrochemical performance of prepared PWGNCs is interesting (PWGNC750: 1200 mA h g^{-1} at 0.2 A g^{-1}; 510 mA h g^{-1} at 5 A g^{-1}). The present study demonstrated only one example as anodes of LIBs for application of the present GNCs. They could have many other applications in wide areas as adsorbents, electrode materials, or energy storage media,[29–33] because they have unique structure and high specific surface area.

Conclusions

In conclusion, PWGNCs were prepared from partially removing doped templates inserted in the graphitic layers of the GNCs. In the thermal pyrolysis of GNCs, N atoms partially replaced C ones in the graphitic shells to *in situ* form doping structure, around which graphitic structure was easily oxidized to create doping templates in acid-treatment. After vacuum heating, ~50% oxygen-containing functional groups (doped templates) was removed and nanopores were equably and efficiently created in the shells of GNCs, leading to their specific surface area and mesopore volume were sharply raised (1100 *vs.* 700 $m^2 g^{-1}$; 1.9 *vs.* 1 $cm^3 g^{-1}$). Such created nanopores could offer much efficient diffusion channels for fast distribution of the electrolyte and Li^+, leading to their hollow inner structure available even at elevated charge/discharge rates, which sharply enhanced performance of PWGNC-based anode with charge–discharge rate increasing (31% increasing: 1200 *vs.* 917 mA h g^{-1} at current density of 0.2 A g^{-1}; 50% increasing: 510 *vs.* 335 mA h g^{-1} at 5 A g^{-1}).

Conflicts of interest

There are no conflicts to declare.

Acknowledgements

This research was supported by Pujiang Talent Project (13PJ1407400) and Funds (14520503100, 15520503400) from science and technology commission of Shanghai municipality, Fund (LM201740) from Shanghai association for the promotion of scientific and technological achievements, Funds from Shanghai institute of technology (J2016-312, XTCX2017-1) and research fund (project #21306113) from the National Natural Science Foundation of China.

References

1 J. R. Dahn, T. Zheng, Y. Liu and J. S. Xue, *Science*, 1995, **270**, 590.
2 G. Li, L. Xu, Q. Hao, M. Wang and Y. Qian, *RSC Adv.*, 2012, **2**, 284.
3 C. Ma, J. Dong, Y. Zhao, J. Li and H. Chen, *Carbon*, 2016, **110**, 180.
4 W. Wang, Y. Sun, B. Liu, S. Wang and M. Cao, *Carbon*, 2015, **91**, 56.
5 J. W. Hu, Z. P. Wu, S. W. Zhong, W. B. Zhang and S. Suresh, *Carbon*, 2015, **87**, 292.
6 G. Maurin, C. Bousquet, F. Henn, P. Bernier, R. Almairac and B. Simon, *Chem. Phys. Lett.*, 1999, **312**, 14.

7 H. Yue, F. Li, Z. B. Yang, J. Tang, X. W. Li and D. Y. He, *Mater. Lett.*, 2014, **120**, 39.
8 P. Han, B. Yang, Z. Qiu, Y. You, J. Jiang, J. Liu, J. Xu, H. Fan and C. Zhu, *RSC Adv.*, 2016, **6**, 7591.
9 Z. S. Wu, W. Ren, L. Xu, F. Li and H. M. Cheng, *ACS Nano*, 2011, **5**, 5463.
10 Z. M. Sheng and J. N. Wang, *Adv. Mater.*, 2008, **20**, 1071.
11 J. Ou, Y. Zhang, L. Chen, Q. Zhao, Y. Meng, Y. Guo and D. Xiao, *J. Mater. Chem. A*, 2015, **3**, 6534.
12 C. Y. Hong, Z. M. Sheng, M. H. Hu, X. Y. Dai, C. K. Chang, Q. Z. Chen and D. Y. Zhang, *RSC Adv.*, 2016, **6**, 59896.
13 R. Mukherjee, A. V. Thomas, A. Krishnamurthy and N. Koratkar, *ACS Nano*, 2012, **6**, 7867.
14 J. Sun, L. Wang, R. Song and S. Yang, *RSC Adv.*, 2015, **5**, 91114.
15 W. Ai, Z. M. Luo, J. Jiang, J. H. Zhu, Z. Z. Du, Z. X. Fan, L. H. Xie, H. Zhang, W. Huang and T. Yu, *Adv. Mater.*, 2014, **26**, 6186.
16 T. Hu, X. Sun, H. Sun, G. Xin, D. Shao, C. Liua and J. Lian, *Phys. Chem. Chem. Phys.*, 2014, **16**, 1060.
17 L. Zhu, H.-J. Peng, J. Liang, J.-Q. Huang, C.-M. Chen, X. Guo, W. C. Zhu, P. Li and Q. Zhang, *Nano Energy*, 2015, **11**, 746.
18 S. Liu, X. Hong, Y. Li, J. Xu, C. Zheng and K. Xie, *RSC Adv.*, 2016, **6**, 98035.
19 C. Tang, B.-Q. Li, Q. Zhang, L. Zhu, H.-F. Wang, J.-L. Shi and F. Wei, *Adv. Funct. Mater.*, 2016, **26**, 577.
20 J. Q. Shan, Y. X. Liu, Y. Z. Su, P. Liu, X. D. Zhuang, D. Q. Wu, F. Zhang and X. L. Feng, *J. Mater. Chem. A*, 2016, **4**, 314.
21 Y. Su, Y. Liu, P. Liu, D. Wu, X. Zhuang, F. Zhang and X. Feng, *Angew. Chem., Int. Ed.*, 2015, **54**, 1812.
22 T. Li, C. Wei, Y.-M. Wu, F.-D. Han, Y.-X. Qi, H.-L. Zhu, N. Lun and Y.-J. Bai, *ACS Appl. Mater. Interfaces*, 2015, **7**, 5107.
23 K. F. Huo, W. L. An, J. J. Fu, B. Gao, L. Wang, X. Peng, G. J. Cheng and P. K. Chu, *J. Power Sources*, 2016, **324**, 233.
24 J. Zhang, L. Zhang, S. Yang, D. Li, Z. Xie, B. Wang, Y. Xia and F. Quan, *J. Alloys Compd.*, 2017, **701**, 256.
25 X. Yang, C. Wei, C. Sun, X. Li and Y. Chen, *J. Alloys Compd.*, 2017, **693**, 777.
26 C. Wang, Y. Huang, H. Pan, J. Jiang, X. Yang, Z. Xu, H. Tian, S. Han and D. Wu, *Electrochim. Acta*, 2016, **215**, 100.
27 H. Sun, Q. Wang, H. Geng, B. Li, Y. Li, Q.-H. Wu, J. Fan and Y. Yang, *Electrochim. Acta*, 2016, **213**, 752.
28 L. Qu, Y. Liu, J.-B. Baek and L. Dai, *ACS Nano*, 2010, **4**, 1321.
29 C. Liu, J. Wang, J. Li, M. Zeng, R. Luo, J. Shen, X. Sun, W. Han and L. Wang, *ACS Appl. Mater. Interfaces*, 2016, **8**, 7194.
30 Z. M. Sheng, C. X. Guo and C. M. Li, *Electrochem. Commun.*, 2012, **19**, 77.
31 Z. M. Sheng, M. H. Hu, X. Y. Dai, C. Y. Hong, C. K. Chang, Q. Z. Chen and X. J. Chang, *Microporous Mesoporous Mater.*, 2016, **234**, 224.
32 W. Lee and J. H. Moon, *ACS Appl. Mater. Interfaces*, 2014, **6**, 13968.
33 Z. Li, L. Ma, T. W. Surta, C. Bommier, Z. Jian, Z. Xing, W. F. Stickle, M. Dolgos, K. Amine, J. Lu, T. Wu and X. Ji, *ACS Energy Lett.*, 2016, **1**, 395.